Check for updates

Adsorption and reduction of hexavalent chromium on magnetic greigite (Fe₃S₄)-CTAB: leading role of Fe(II) and S(−II)†

Yanxia Zhou,[a] Yiting Zhao,[a] Xiaoge Wu,[a] Weiqin Yin,[a] Jianhua Hou, [ID][ab]
Shengsen Wang,[ab] Ke Feng[ab] and Xiaozhi Wang [ID] *[abc]

In this study, a facile one-step route was used to synthesize a novel magnetic mesoporous greigite (Fe₃S₄)-CTAB composite, which was utilized to remove hexavalent chromium (Cr(VI)). The optimized Fe₃S₄-CTAB$_{0.75}$ composite with a CTAB dosage of 0.75 g possessed the maximum specific surface, showing the highest Cr(VI) adsorption capacity of 330.03 mg g^{-1}. The mechanism analysis revealed that Fe(II) and S(−II) were critical for the reduction of Cr(VI). CTAB can promote the removal of Cr(VI) by Fe₃S₄-CTAB composites, possibly due to increased S(−II) concentration, better dispersion of nanoparticles, and greater zeta potential. Besides, there is mild effect of Fe⁰ on Cr(VI) removal, which is confirmed by the disappearance of the Fe⁰ peak from the XPS analysis. The pseudo-second-order kinetic model could explain the Cr(VI) removal processes well. The adsorption of Cr(VI) at different initial concentrations was more consistent with a Langmuir isotherm. The existence of H⁺ was beneficial for Cr(VI) removal by Fe₃S₄-CTAB$_{0.75}$. Our work confirmed that the obtained Fe₃S₄-CTAB$_{0.75}$ composites exhibit considerable potential for Cr(VI) removal from aqueous solution.

1. Introduction

As a metal contaminant, chromium frequently occurs in wastewater. Since it could seriously harm human health, the U.S. Environmental Protection Agency (EPA) has listed hexavalent chromium as a group 'A' human carcinogen.[1] Cr(III) and Cr(VI) are the most common and stable forms of chromium,[2,3] and the poisonousness of the latter is 100 times larger than the former.[4] It has been reported that long exposure to Cr(VI) could induce many diseases, for example liver failure, reproductive failure, chronic headaches, respiratory disease, nose bleeds and any type of cancer.[5]

A lot of technologies have been utilized to remove Cr(VI) from the environment, such as photoreduction,[6,7] electro-chemical precipitation,[8] ion exchange,[9] and adsorption.[10] Combining with adsorption, chemical reduction from Cr(VI) to Cr(III) to reduce toxicity is one of the most simple and economical methods.[11] The combined strategy includes many advantages, such as high efficiency, easy use, and low cost.[12]

Greigite (Fe₃S₄) is isostructural with Fe₃O₄.[13–15] Due to its low cost and good chemical reduction ability, Fe₃S₄ has been applied on heavy metal removal.[12] For example, Kong and his coworkers investigated lead (Pb²⁺) transformations on β-cyclodextrin stabilized magnetic Fe₃S₄ nanoparticles, and found that the surface adsorption and chemical precipitation (PbS) were the dominant mechanisms in the process of removing lead.[16] Mahamudur Islam *et al.* utilized greigite-conducting polypyrrole nanocomposite to remove arsenate and arsenite from aqueous solution.[17] However, the application of Fe₃S₄ in the adsorption and reduction of hexavalent chromium is rarely investigated. According to the previous reports,[18] Fe₃S₄ can release Fe(II) and S(−II) in aqueous solution, which can promote Cr(VI) reduction effectively.

Various cationic surfactants have been applied to removal anionic metal.[19] Appropriate surfactants or stabilizers such as β-CD, PEG, and CTAB, could affect the purity and stability of Fe₃S₄.[20] Cetyltrimethylammonium bromide (CTAB) is one of the common cationic surfactants and it is known that the dissociated cetyltrimethylammonium (CTA⁺) maintains the properties of surfactant. CTAB could help to obtain high purity greigite microcrystals,[21] improve the content of S(−II) in greigite, and CTA⁺ could combine with Cr(VI) anions and form ion-pairs.[22] This is the first work about the application of Fe₃S₄-CTAB to removal Cr(VI).

The task of this study was to prepare greigite (Fe₃S₄) doped with CTAB for the removal of Cr(VI). The detailed works were listed as following: (1) synthesize and characterize greigite

[a]College of Environmental Science and Engineering, Yangzhou University, Jiangsu 225127, China. E-mail: xzwang@yzu.edu.cn

[b]Jiangsu Collaborative Innovation Center for Solid Organic Waste Resource Utilization, Nanjing 210095, China

[c]Institutes of Agricultural Science and Technology Development, Yangzhou University, Yangzhou 225127, Jiangsu, China

† Electronic supplementary information (ESI) available. See DOI: 10.1039/c8ra06534a

(Fe_3S_4) doped with CTAB, (2) determine the effects of solution pH, reaction time, CTAB doping amount, and initial concentrations of contaminant on the Cr(VI) removal effectiveness, (3) investigate the reductive and adsorptive capacity of Cr(VI). This work could provide evidence to explain Cr(VI) removal mechanisms by Fe_3S_4-CTAB.

2. Materials and methods

2.1 Chemical reagents

$K_2Cr_2O_7$ was dissolved to prepare Cr(VI) stock solutions. Ferric chloride hexahydrate ($FeCl_3 \cdot 6H_2O$), thiourea, ethylene glycol (EG), ethanol, potassium dichromate ($K_2Cr_2O_7$), cetyltrimethylammonium bromide (CTAB) were purchased from Yangzhou Chemicals Corporation (Yangzhou, China). Solution pH was regulated by 1 M HCl and/or NaOH. Deionized water was used in the whole experiment. All reagents used were of analytical grade and had not been further purified before use.

2.2 Synthesis of greigite and greigite-CTAB composite

Fe_3S_4 composite was synthesized by the modified hydrothermal method.[18] Briefly, $FeCl_3 \cdot 6H_2O$ (3.0 mmol) and thiourea (6.0 mmol) were added to EG (60 mL) and stirred for 20 min to form a carmine solution. Typically, CTAB (0.75 g) was then added to the carmine solution, followed by 15 min magnetic stirring and 15 min sonication. After the mixing, the above solution was transferred into a autoclave (the capacity is 100 mL). After 12 h heating at 180 °C, a magnet was used to collect solid products. The collected samples were repeatedly washed with distilled water followed by ethanol. The obtained $Fe^0/FeS/Fe_3S_4$-$CTAB_{0.75}$ (referred to as Fe_3S_4-$CTAB_{0.75}$ in the article) were dried in a vacuum oven at 60 °C for 12 h. Following the similar fabricated method, other Fe_3S_4-CTAB samples were prepared with varying amounts of CTAB and named as Fe_3S_4-$CTAB_{0.25}$, Fe_3S_4-$CTAB_{0.50}$, and Fe_3S_4-$CTAB_{1.00}$.

2.3 Batch experiments of Cr(VI) removal

In order to determine the best pH in the reaction process, the pH value of the Cr(VI) solutions was set to 2.0, 3.0, 4.0, 5.0 and 6.0, respectively, with 1 M HCl and 1 M NaOH. Typically, the obtained composite (15 mg) was mixed with Cr(VI) solution (50 mL of 100 mg L^{-1}), and then continuously shaken for 1 h at room temperature. The experimental data of adsorption kinetic was obtained by sampling at certain time intervals, then the suspension was filtered through a 0.22 mm membrane to achieve clarified samples. Adsorption isotherms were performed by mixing the composite with Cr(VI) solution (initial concentration ranging from 100 to 300 mg L^{-1}) and shaking for 5 h to obtain adsorptive equilibrium.

2.4 Analysis

Total Cr(VI) in solution was confirmed through the 1,5-diphenylcarbazide colorimetric method (with potassium permanganate).[23] Moreover, the 1,5-diphenylcarbazide colorimetric method was applied to measure the Cr(VI) concentrations at 540 nm through a UV/Vis spectrophotometer.[24] The Cr(III)

concentration corresponded to the difference between total Cr and Cr(VI). The Cr speciation of the reaction product was confirmed by XPS.[2] The o-phenanthroline method was utilized to determine the concentration of ferrous ions at 510 nm. Through adding hydroxylamine hydrochloride to reduce Fe from Fe(III) to Fe(II), then the total dissolved iron was measured.[24]

2.5 Characterization

XRD analysis (D8 Advance Bruker AXS, Germany) was applied to determine the phase structure of the obtained composites. HRTEM was obtained using a Tecnai G2 F30 S-TWIN (FEI, USA) to ensure the crystal lattice of the reaction product. Scanning electron microscope (S-4800II, Japan) was used to observe the surface morphology of the obtained composite. Fourier transform infrared (FTIR) spectra were obtained by using a Thermo Nicolet iS5 spectrometer, using KBr as a reference. The magnetization of the obtained composites was obtained on a vibrating sample magnetometry (VSM-EV7, ADE). Micromeritics ASAP 2460 was applied to confirmed nitrogen adsorption–desorption isotherms and specific surface areas. The valence state of related elements of the adsorbent before and after reaction was identified by XPS (ESCALAB 250 Xi, USA). Zeta potentials of the obtained composites were measured through zeta potentiometer (DTS1060).

3. Results and discussion

3.1 Characterization of greigite and greigite-CTAB composite

The crystal structure and phase purity of the obtained composites and Cr(VI)-treated Fe_3S_4-$CTAB_{0.75}$ were determined by XRD pattern. From Fig. 1, FeS shows three 2θ peaks at 17.61°, 38.99° and 49.59°, which correspond to [001], [111] and [200] directions. The other diffraction peaks can correspond well to cubic Fe_3S_4 (JCPDS file no. 89-1998).[17] No other impurity peaks were observed between bare Fe_3S_4 and CTAB modified Fe_3S_4 composite, indicating that the existence of CTAB did not change the structure of Fe_3S_4. Meanwhile, the product from the reaction of Fe_3S_4-$CTAB_{0.75}$ with Cr(VI) was shown in Fig. 1. The XRD pattern showed that the diffraction peaks of FeS disappeared and a new diffraction peak attributed to Cr_2O_3 emerged.
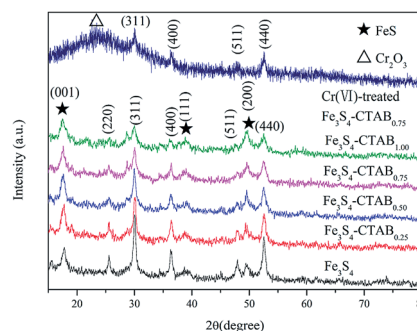

Fig. 1 XRD patterns of Fe_3S_4, Fe_3S_4-$CTAB_{0.25}$, Fe_3S_4-$CTAB_{0.50}$, Fe_3S_4-$CTAB_{0.75}$, Fe_3S_4-$CTAB_{1.00}$ and Cr(VI)-treated Fe_3S_4-$CTAB_{0.75}$.

HRTEM (Fig. S1†) was applied to determine the composition of Cr(VI)-treated Fe_3S_4-$CTAB_{0.75}$. The *d*-spacing in HRTEM was about 0.25 nm and 0.334 nm in accordance with the (110) faces of Cr_2O_3 and $Cr(OH)_3$ respectively,[25,26] which demonstrated the existence of Cr_2O_3 and $Cr(OH)_3$.

SEM images under high magnification (Fig. S2†) clearly displayed that a large amount of nanosheets formed 3D flower-shaped microspheres, which agreed with previous reports.[18] The FTIR spectra of the obtained composites and pure CTAB were presented in Fig. S3.† Interestingly, the peaks at 2400 cm^{-1} and 2300 cm^{-1} became more obvious with the increase of CTAB doping amount. These coincided with the spectra of pure CTAB between 2400 cm^{-1} and 2300 cm^{-1} indicating Fe_3S_4 crystals doped with CTAB has been successfully fabricated.

The magnetization of obtained composites were gained under the condition of an applied magnetic field. The magnetic hysteresis loop of the obtained Fe_3S_4, Fe_3S_4-$CTAB_{0.25}$, Fe_3S_4-$CTAB_{0.50}$, Fe_3S_4-$CTAB_{0.75}$ and Fe_3S_4-$CTAB_{1.00}$ were shown in Fig. 2, which indicates that all the five composites exhibit ferromagnetic nature. The saturation magnetization of greigite-CTAB composite decreased gradually due to the attachment of nonmagnetic component.

The nitrogen adsorption–desorption method were applied to determine the specific surface area of the obtained composites. A type IV isotherm shown in Fig. S4† displayed the presence of mesopores structure. Table 1 summarizes the BET surface area of the obtained composites with varied doping amount of CTAB. Fe_3S_4 has a specific surface of 18.82 $m^2\ g^{-1}$. With the increase of doping amount of CTAB, the surface area of the obtained composites decreases first and then increases. When CTAB doping increases to 0.75 g, the highest BET surface area is obtained. When the CTAB content is low, it will adsorb on the pore surfaces, leading to the reduction of the pore size and specific surface areas.[27] But when we increase CTAB dosage, it acts as a mesopore directing agent,[28] which will enter into the material structure, thus increasing the specific surface area of the material.[29]

XPS spectroscopy was used to examine the valence change of related elements before and after treatment of Cr(VI) (Fig. 3). For Fe_3S_4-$CTAB_{0.75}$, the Fe 2p spectra in Fig. 3(a) was decomposed to
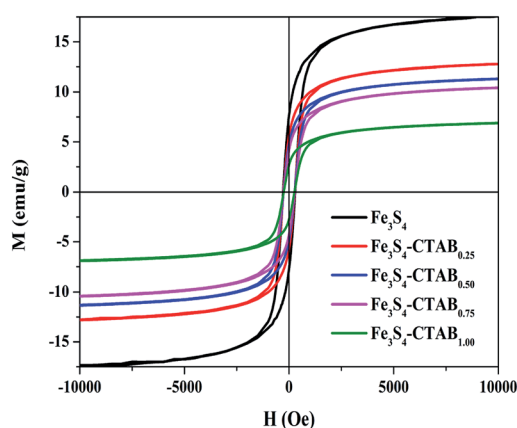
Table 1 Surface area, average pore size and pore volume of Fe_3S_4, Fe_3S_4-$CTAB_{0.25}$, Fe_3S_4-$CTAB_{0.50}$, Fe_3S_4-$CTAB_{0.75}$ and Fe_3S_4-$CTAB_{1.00}$ composites

Sample	S_{BET} ($m^2\ g^{-1}$)	Average pore size (nm)	Pore volume ($cm^3\ g^{-1}$)
Fe_3S_4	18.82	15.035	0.071
Fe_3S_4-$CTAB_{0.25}$	15.13	6.934	0.026
Fe_3S_4-$CTAB_{0.50}$	16.69	15.799	0.066
Fe_3S_4-$CTAB_{0.75}$	21.27	14.895	0.079
Fe_3S_4-$CTAB_{1.00}$	20.95	6.116	0.032

five peaks. The binding energies of Fe(II) were at 707.6 (ref. 30) and 710.3 eV.[24,31] The Fe peak at 2p3/2 = 720.2 eV which can be assigned to Fe^0.[32,33] The binding energies of Fe 2p3/2 and Fe 2p1/2 are at 713.3 eV and 724.4 eV, respectively, proving of the existence of Fe(III).[32,34] The S 2p spectra in Fig. 3(b) exhibited five peaks, namely, FeS at about 161 (ref. 31) and 162 (ref. 24) eV, S(−I) at about 163 eV,[35] S(VI) at about 168 eV.[24,36] The O 1s was decomposed into different peaks at binding energies of 530 eV and 531 eV, consisting with O^{2-} (ref. 30) and C–O,[31] respectively. Furthermore, the proportion of the reduced sulfur in Fe_3S_4-$CTAB_{0.75}$ was increased and the diffraction peak –OH was converted into C–O after CTAB doping (Fig. S5†). These changes further proved that CTAB had been successfully doped into greigite.

Upon Cr(VI) sorption, the reductive state of iron(Fe(II) and Fe^0) decreased from 59.84% for Fe_3S_4-$CTAB_{0.75}$ to 49.85% for Cr(VI)-spent Fe_3S_4-$CTAB_{0.75}$, whereas Fe(III) increased from 40.16% to 50.15% (Table S1†). Furthermore, the peak assigned to Fe^0 disappeared, while a new peak ascribed to Fe(III) appeared at 718.9 eV.[37] It displays the oxidation of Fe(II) and Fe^0 by Cr(VI) under the condition of experiment. The percentage of S(−II) decreased from 47.36% to 24.25%, and S(VI) increased from 11.13% to 27.57% after contacting with Cr(VI) (Table S1†), revealing the oxidization of S(−II) by Cr(VI). The peak assigned to
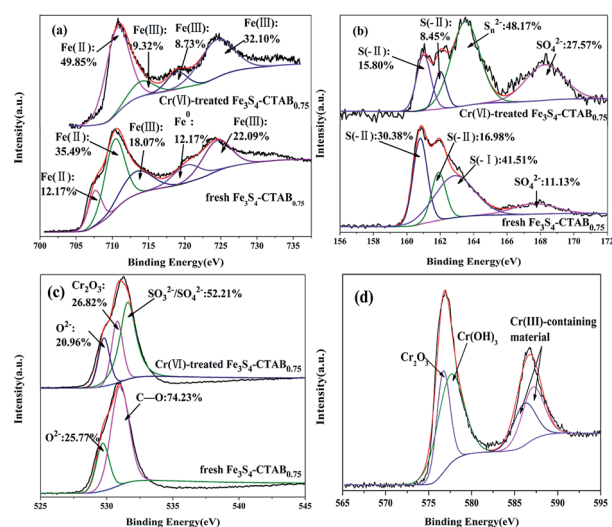

Fig. 2 Hysteresis (M−H) analysis of Fe_3S_4, Fe_3S_4-$CTAB_{0.25}$, Fe_3S_4-$CTAB_{0.50}$, Fe_3S_4-$CTAB_{0.75}$ and Fe_3S_4-$CTAB_{1.00}$.

Fig. 3 XPS spectra of (a) the Fe 2p region, (b) the S 2p region, (c) the O 1s region and (d) the Cr 2p region of the fresh and Cr-treated Fe_3S_4-$CTAB_{0.75}$ sample.
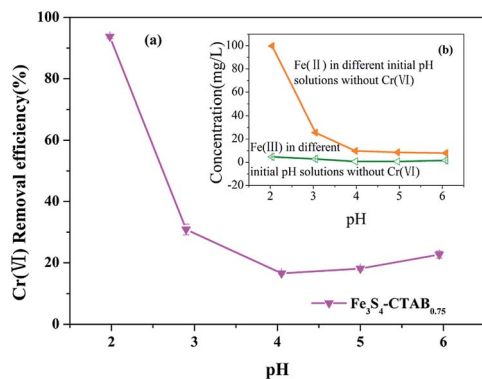
Fig. 4 (a) Effects of initial solution pHs on Cr(VI) removal efficiency (initial Cr(VI) concentration = 100 mg L^{-1}; Fe$_3$S$_4$-CTAB$_{0.75}$ dosage = 0.3 g L^{-1}). (b) The concentration of dissolved Fe(II) and Fe(III) from Fe$_3$S$_4$-CTAB$_{0.75}$ in solution with different initial pHs without Cr(VI).

S(−I) vanished, indicating it could react with Fe(III) to form Fe(II) and release H$^+$ (FeS$_2$ + 14Fe^{3+} + 8H$_2$O → 15Fe^{2+} + 2SO$_4^{2-}$ + 16H$^+$).[38] Simultaneously, a new peak ascribed to S$_n^{2-}$ ($n > 2$) resulting from the oxidation of FeS and/or FeS$_2$ (ref. 39) appeared at 163.5 eV.[30,34] For O 1s, C–O disappeared, the binding energy at 531.6 eV suggests the existence of SO$_3^{2-}$/SO$_4^{2-}$,[30] which is consistent with the increased proportion of S(VI). Additionally, a new peak assigned to Cr$_2$O$_3$ emerged at 530.8 eV (ref. 31) supported by the XRD of Cr(VI)-treated Fe$_3$S$_4$-CTAB$_{0.75}$. Chromium species were determined via the high-resolution XPS Cr 2p spectrum (Fig. 3(d)). The Cr 2p3/2 signal of Cr(VI)-treated Fe$_3$S$_4$-CTAB$_{0.75}$ was partitioned into two contributions: the binding energy at 576.7 eV and 577.5 eV are assigned to Cr$_2$O$_3$ (ref. 40) and Cr(OH)$_3$,[40,41] respectively. The results are consistent with the observation from HRTEM. The binding energies of Cr 2p1/2 (586.1 eV and 587.1 eV) were close to those of Cr(III)-containing material.[42,43]

3.2 Effect of pH on Cr(VI) removal

Solution pH is a critical parameter in the process of adsorption and reduction of Cr(VI).[44] As shown in Fig. 4(a), the removal efficiency of Cr(VI) in the solution was 93.73% and 22.67%, respectively, corresponding to the pH value of 2.0 and 6.0. Under the pH range from 2.0 to 4.0, the removal efficiency of Cr(VI) showed a significant drop, which is consistent with

previous experimental results.[45] This trend coincided with the marked decrease of concentration of dissolved Fe(II) from Fe$_3$S$_4$-CTAB$_{0.75}$ (Fig. 4(b)). The result may suggest facilitated dissolution of Fe^{2+} at lower pHs played important roles in Cr(VI) removal. Besides, the isoelectric point of the material is between pH 2.0 and 3.0,[46] and thus material becomes positively charged and protonated at pH 2.0 which is favourable for electrostatic attraction between HCrO$_4^-$.[47] This was also further confirmed with positive zeta potential at pH 2.0 (Fig. S6†). However, higher pH values will change the surface charge of the material, impairing the electrostatic attraction between the material and Cr(VI) anions. Furthermore hydroxyls from the higher pH value solution could compete the adsorption sites on Fe$_3$S$_4$-CTAB$_{0.75}$ surface with Cr(VI) anions, leading to a reduction of the removal efficiency of Cr(VI).[22] However, under the pH range from 4.0 to 6.0, the removal efficiency slightly increased, which may be due to the formation of a small amount of Cr(OH)$_3$.[48] In addition, coexistence of H$^+$ at lower pH and reduced sulphur was able to reduce Cr(VI) to Cr(III) more easily.[49] Based on the pH-dependent sorption of Fe$_3$S$_4$-CTAB, we choose the pH valve at 2.0 for further removal studies.

3.3 Effects of CTAB dosage on Cr(VI) removal kinetics

Fig. 5(a) shows the adsorption data of Cr(VI) at different time intervals. The initial concentration of Cr(VI) was set to 100 mg L^{-1} and the amount of Fe$_3$S$_4$-CTAB$_X$ (initial pH = 2.0) added was 0.3 g L^{-1}. It can be seen that adsorption reached equilibrium after 30 min reaction. The removal effectiveness of Fe$_3$S$_4$-CTAB$_X$ is affected by the amount of CTAB doping. Cr(VI) removal efficiency was about 70% and 94% for Fe$_3$S$_4$ and Fe$_3$S$_4$-CTAB$_{0.75}$ after 60 min, respectively. The enhanced removal of Cr(VI) by CTAB composites might be attributed to several reasons. First, the higher reduced sulfur in the composites as revealed by the XPS analysis (Fig. S5(a)†) facilitated its reduction reaction with Cr(VI). This could be a very important mechanism associated with our composites. Second, the CTAB improved the dispersion and reduced the aggregation of Fe$_3$S$_4$ to Cr(VI) (Fig. S2(a) & (d)†). Third, the cationic surfactant CTAB could increase electrostatic attraction with negatively charged HCrO$_4^-$ on one hand. On the other hand, CTAB could increase zeta potential of Fe$_3$S$_4$ compared to pristine Fe$_3$S$_4$ which provide more positive surface for attraction with HCrO$_4^-$ at
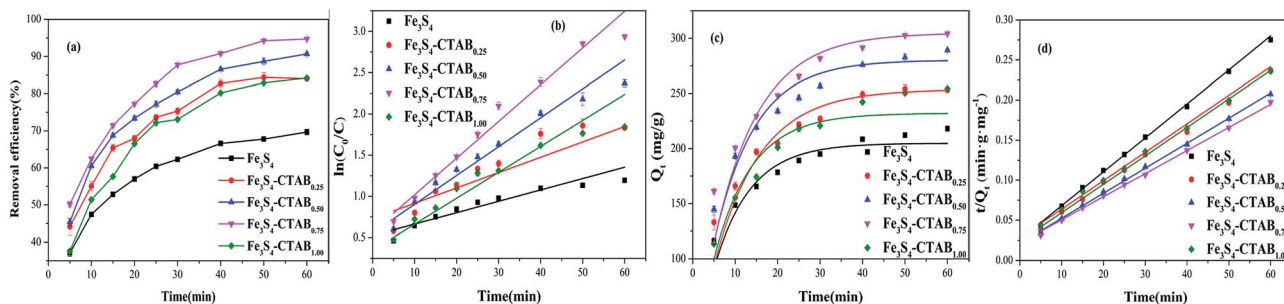

Fig. 5 (a) Comparative experiments among Fe$_3$S$_4$, Fe$_3$S$_4$-CTAB$_{0.25}$, Fe$_3$S$_4$-CTAB$_{0.50}$, Fe$_3$S$_4$-CTAB$_{0.75}$ and Fe$_3$S$_4$-CTAB$_{1.00}$ at pH 2.0 (reaction conditions: 0.3 g L^{-1} synthesis, 100 mg L^{-1} Cr(VI)). (b) Pseudo-first-order reaction model corresponding to (a). (c) Pseudo-first-order adsorption model corresponding to (a). (d) Pseudo-second-order adsorption model corresponding to (a).

Table 2 Adsorption kinetics parameters for the adsorption of Cr(VI)

Sample	Pseudo-first-order model			Pseudo-second-order model		
	K_1 (min^{-1})	Q_e (mg g^{-1})	R^2	$K_2 \times 10^{-4}$ (g (mg min)$^{-1}$)	Q_e (mg g^{-1})	R^2
Fe_3S_4	0.117	204.925	0.883	7.023	235.849	0.998
Fe_3S_4-CTAB$_{0.25}$	0.092	253.764	0.941	5.302	281.690	0.999
Fe_3S_4-CTAB$_{0.50}$	0.105	280.186	0.908	4.659	319.489	0.998
Fe_3S_4-CTAB$_{0.75}$	0.094	304.922	0.977	3.881	346.021	0.999
Fe_3S_4-CTAB$_{1.00}$	0.113	232.121	0.924	4.491	280.899	0.997

experimental pH (Fig. S6†). As shown in Table 2, the pseudo second-order adsorption model was more suitable than the pseudo first-order adsorption model to explain Cr(VI) removal from correlation coefficients. Thus, the difference in the removal rate by obtained composites is expressed by the pseudo first-order reaction model (Fig. 5(b)). The kinetic parameters calculated from the pseudo-first reaction model are listed in Table S2,† where reaction rate of Fe_3S_4-CTAB$_{0.75}$ is 3–4 times greater than pristine Fe_3S_4.

To gain a better explanation of transformation of chromium species, the total chromium concentrations were examined at different sampling time points (shown in Fig. 6). The total chromium concentration dropped sharply within 5 min, and then gradually reached equilibrium within 30 min. The residual total chromium concentration dropped to 40 mg L^{-1} at 60 min, about 85% of the chromium was Cr(III), which is less toxic than Cr(VI). Therefore, it is suggested that Cr(VI) could be reduced to Cr(III) effectively by Fe_3S_4-CTAB$_{0.75}$.

3.4 Adsorption isotherm

The adsorption isotherm of Cr(VI) removal was discussed by changing the initial concentrations of contaminant, with the Fe_3S_4-CTAB$_{0.75}$ dosage of 0.3 g L^{-1} (initial pH = 2.0). The related model parameters were shown in Table S1.† The adsorption capacity of Fe_3S_4-CTAB$_{0.75}$ reached to 303.53 mg g^{-1} and 329.95 mg g^{-1} with initial Cr(VI) concentrations of 100 and 300 mg L^{-1}, respectively. The Freundlich model could not fit the experimental data well (Fig. S7†), compared with the Langmuir model ($R^2 = 0.99$) (Fig. 7).

According to the fitting results, it could be speculated that the adsorption of Cr(VI) by Fe_3S_4-CTAB$_{0.75}$ was mononuclear layer adsorption.[24] The calculated Q_{max} value (the adsorption capacity) was 330.03 mg g^{-1}. Fe_3S_4-CTAB$_{0.75}$ exhibited a excellent removal good capacity for Cr(VI), compared with other Fe-based adsorbents (Table 3).

3.5 Proposed Cr(VI) removal mechanism

Based on the above discussion, a possible mechanism for Cr(VI) removal on Fe_3S_4-CTAB$_{0.75}$ was preliminarily proposed as follows. The mesoporous Fe_3S_4-CTAB$_{0.75}$ composite could adsorb Cr(VI) rapidly as CTA$^+$ cations can combine the HCrO$_4^-$ (main species of hexavalent chromium at pH 2.0 (ref. 41)) to form ion-pairs (eqn (1)).[22] Moreover Fe^0 could be easily oxidized by Cr(VI).[32] The absorbed Cr(VI) is *in situ* reduced by Fe^0 to generate Cr(III), accompanied by the oxidation of Fe^0 to form Fe(II),[51] which is consistent with the disappearance of Fe^0 peak (Fig. 3(b)) (eqn (2)). Furthermore, dissolved FeS provides Fe(II) and S(−II) (eqn (3)) donating the electrons to Cr(VI),[31,38] which was evidenced by the increase of SO$_4^{2-}$ content in Fig. 3(b) (eqn (4)). In addition, we measured the concentration of Fe(II) and Fe(III) in deionized water (pH = 2.0) and in the presence of Cr(VI) (pH = 2.0) at different time intervals, respectively. Without
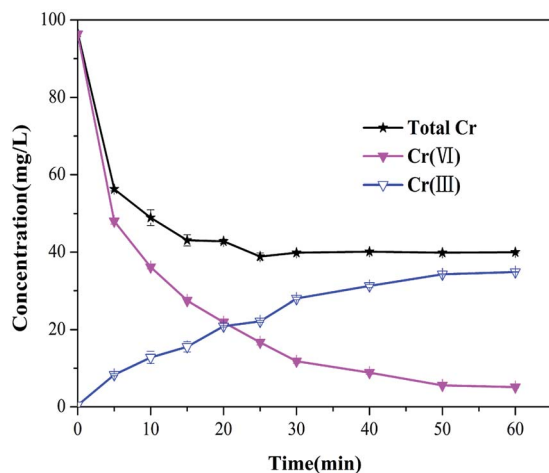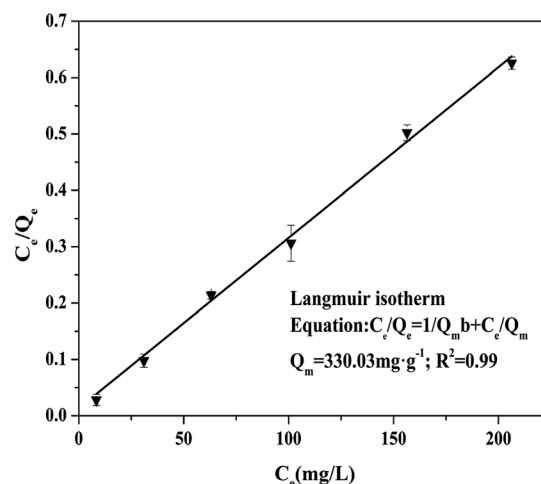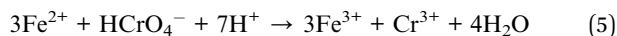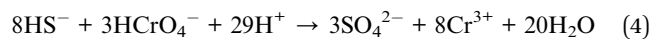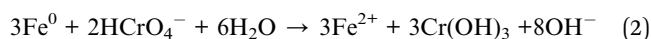

Fig. 6 Concentrations of the total chromium, Cr(III) and Cr(VI) in the solution during the Cr(VI) transformation by Fe_3S_4-CTAB$_{0.75}$ remaining in the solution (C_0 = 100 mg L^{-1}, pH = 2.0, Fe_3S_4-CTAB$_{0.75}$ dosage = 0.3 g L^{-1}), the corresponding Cr(III) and Cr(VI).
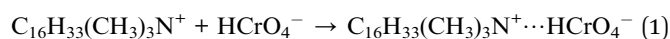

Fig. 7 Langmuir isotherm of Cr(VI) adsorption. The reactions were developed at initial Cr(VI) concentrations of 100−300 mg L^{-1} with 0.3 g L^{-1} Fe_3S_4-CTAB$_{0.75}$, with pH$_0$ = 2.0.

Table 3 Comparison of the maximum Cr(VI) adsorption capacity of various adsorbents

Adsorbents	S_{BET} (m^2 g^{-1})	q_m (mg g^{-1})	pH	Equilibrium time (h)	Ref.
FeS@Fe^0	53.11	66.7	5.0	2	24
FeS-coated iron (Fe/FeS)	62.1	69.7	5.0	72	38
CMC-FeS@biochar	51.5	130.5	5.5	72	31
FeS	—	240	5	4.5	50
MnFe$_2$O$_4$@SiO$_2$-CTAB	53.4	25.044	3.0	12	22
Fe$_3$O$_4$ capped with CTAB	—	10.05	4.0	12	19
Fe$_3$S$_4$-CTAB$_{0.75}$	21.273	330.03	2.0	1	This study
		76.65	6.0		

Cr(VI), dominant iron species in acidic solution (pH = 2.0) is in the Fe(II) state, while after 60 min reaction in the presence of Cr(VI), iron exists mainly in trivalent iron(Fig. S8†). Thus, it is suggested that Cr(VI) is reduced by ferrous ions dissolved from Fe$_3$S$_4$-CTAB$_{0.75}$ (eqn (5)).[2,52]

$$C_{16}H_{33}(CH_3)_3N^+ + HCrO_4^- \rightarrow C_{16}H_{33}(CH_3)_3N^+ \cdots HCrO_4^- \quad (1)$$

$$3Fe^0 + 2HCrO_4^- + 6H_2O \rightarrow 3Fe^{2+} + 3Cr(OH)_3 + 8OH^- \quad (2)$$

$$FeS + H^+ \rightarrow Fe^{2+} + HS^- \quad (3)$$

$$8HS^- + 3HCrO_4^- + 29H^+ \rightarrow 3SO_4^{2-} + 8Cr^{3+} + 20H_2O \quad (4)$$

$$3Fe^{2+} + HCrO_4^- + 7H^+ \rightarrow 3Fe^{3+} + Cr^{3+} + 4H_2O \quad (5)$$

4. Conclusions

Novel greigite-CTAB composites applied to remove Cr(VI) from aqueous solutions were successfully synthesized by a simple one-step modification method. The effectiveness of greigite-CTAB composites varies with the doping content of CTAB. When the doping content of CTAB was 0.75 g, the highest Cr(VI) removal capacity was achieved. Langmuir isotherm model matches better than Freundlich isotherm model in fitting Cr(VI) adsorption datas. The predicted maximum Cr(VI) removal capacity is 330.03 mg g^{-1}. The removal process is in accordance with pseudo-second-order kinetic model. Furthermore, low pH value of the system is crucial to the reduction of Cr(VI) to Cr(III). It could be inferred that the release of Fe(II) under acidic conditions is favorable. In the case of Fe$_3$S$_4$-CTAB$_{0.75}$, Cr(VI) was adsorbed on the adsorbent surface through electrostatic attraction followed by reduced to less toxic Cr(III). Therefore, the novel greigite-CTAB composites have great potential for the efficient removal of Cr(VI) in wastewater.

Conflicts of interest

There are no conflicts to declare.

Acknowledgements

References

1 B. Dhal, H. N. Thatoi, N. N. Das and B. D. Pandey, *J. Hazard. Mater.*, 2013, **250–251**, 272–291.

2 T. Yang, L. Meng, S. Han, J. Hou, S. Wang and X. Wang, *RSC Adv.*, 2017, **7**, 34687–34693.

3 L. Hua, Y. C. Chan, Y. P. Wu and B. Y. Wu, *J. Hazard. Mater.*, 2009, **163**, 1360–1368.

4 C. Liu, N. Fiol, I. Villaescusa and J. Poch, *Sci. Total Environ.*, 2016, **541**, 101–108.

5 G. R. Xu, J. N. Wang and C. J. Li, *Chem. Eng. J.*, 2012, **198–199**, 310–317.

6 F. Xu, R. D. Webster, J. Chen, T. T. Y. Tan, H. L. Sit and W. Y. Teoh, *Appl. Catal., B*, 2017, **210**, 444–453.

7 Y. Zhang, M. Xu, H. Li, H. Ge and Z. Bian, *Appl. Catal., B*, 2017, **226**, 213–219.

8 C. Peng, H. Meng, S. Song, S. Lu and A. Lopez-Valdivieso, *Sep. Sci. Technol.*, 2005, **39**, 1501–1517.

9 Y. Xing, A. Xueming Chen and D. Wang, *Environ. Sci. Technol.*, 2007, **41**, 1439–1443.

10 K. Parida, K. G. Mishra and S. K. Dash, *J. Hazard. Mater.*, 2012, **241–242**, 395–403.

11 H. Gu, S. Rapole, Y. Huang, D. Cao, Z. Luo, S. Wei and Z. Guo, *J. Mater. Chem. A*, 2013, **1**, 2011–2021.

12 L. Kong, Z. Li, X. Huang, S. Huang, H. Sun, M. Liu and L. Li, *J. Mater. Chem. A*, 2017, **5**, 19333–19342.

13 Y. S. Chang, S. Savitha, S. Sadhasivam, C. K. Hsu and F. H. Lin, *J. Colloid Interface Sci.*, 2011, **363**, 314–319.

14 S. Huang, D. Kang, X. Wu, J. Niu and S. Qin, *Sci. Rep.*, 2017, **7**, 46334.

15 Y. J. Choe, J. Y. Byun, S. H. Kim and J. Kim, *Appl. Catal., B*, 2018, **233**, 272–280.

16 L. Kong, L. Yan, Z. Qu, N. Yan and L. Li, *J. Mater. Chem. A*, 2015, **3**, 15755–15763.

17 M. Islam and R. Patel, *Sep. Sci. Technol.*, 2017, **52**, 2837–2854.

18 W. Liu, Z. Ai, R. A. Dahlgren, L. Zhang and X. Wang, *Chem. Eng. J.*, 2017, **330**, 1232–1239.

19 S. A. Elfeky, S. E. Mahmoud and A. F. Youssef, *J. Adv. Res.*, 2017, **8**, 435–443.

20 M. Feng, Y. Lu, Y. Yang, M. Zhang, Y. J. Xu, H. L. Gao, L. Dong, W. P. Xu and S. H. Yu, *Sci. Rep.*, 2013, **3**, 2994.

21 G. Li, B. Zhang, F. Yu, A. A. Novakova, M. S. Krivenkov, T. Y. Kiseleva, L. Chang, J. Rao, A. O. Polyakov and G. R. Blake, *Chem. Mater.*, 2014, **26**, 5821–5829.

22 L. Na, F. Fu, J. Lu, Z. Ding, T. Bing and J. Pang, *Environ. Pollut.*, 2016, **220**, 1376–1385.

23 S. C. Ponce, C. Prado, E. Pagano, F. E. Prado and M. Rosa, *Ecol. Eng.*, 2015, **74**, 33–41.

24 J. Du, J. Bao, C. Lu and D. Werner, *Water Res.*, 2016, **102**, 73–81.

25 H. Sun, L. Wang, D. Chu, Z. Ma and A. Wang, *Mater. Lett.*, 2015, **140**, 35–38.

26 J. Wu, X. B. Wang and R. J. Zeng, *J. Hazard. Mater.*, 2017, **333**, 275–284.

27 Y. F. Lin and S. H. Hsu, *J. Colloid Interface Sci.*, 2017, **485**, 152–158.

28 G. Qi, Y. Wang, L. Estevez, X. Duan, N. Anako, A. H. A. Park, W. Li, C. W. Jones and E. P. Giannelis, *Energy Environ. Sci.*, 2011, **4**, 444–452.

29 Y. Jiang, W. Wang, X. Li, X. Wang, J. Zhou and X. Mu, *ACS Appl. Mater. Interfaces*, 2013, **5**, 1913–1916.

30 W. Han and M. Gao, *Cryst. Growth Des.*, 2008, **8**, 1023–1030.

31 H. Lyu, J. Tang, Y. Huang, L. Gai, E. Y. Zeng, K. Liber and Y. Gong, *Chem. Eng. J.*, 2017, **322**, 516–524.

32 G. Bing, Z. H. Jin, T. L. Li and X. H. Qi, *Chemosphere*, 2009, **75**, 825–830.

33 S. K. Singh, A. K. Singh, K. Aranishi and Q. Xu, *J. Am. Chem. Soc.*, 2011, **133**, 19638–19641.

34 V. L. Tauson, R. G. Kravtsova, V. I. Grebenshchikova, E. E. Lustenberg and S. V. Lipko, *Geochem. Int.*, 2009, **47**, 231–243.

35 D. C. Frost, W. R. Leeder, R. L. Tapping and B. Wallbank, *Fuel*, 1977, **56**, 277–280.

36 C. Domínguez, F. J. Pérez-Alonso, J. L. G. D. L. Fuente, S. A. Al-Thabaiti, S. N. Basahel, A. O. Alyoubi, A. A. Alshehri, M. A. Peña and S. Rojas, *J. Power Sources*, 2014, **271**, 87–96.

37 T. Mayer, *Appl. Surf. Sci.*, 2001, **179**, 257–262.

38 Y. Gong, L. Gai, J. Tang, J. Fu, Q. Wang and E. Y. Zeng, *Sci. Total Environ.*, 2017, **595**, 743–751.

39 H. W. Nesbitt and I. J. Muir, *Geochim. Cosmochim. Acta*, 1994, **58**, 4667–4679.

40 Q. Liu, M. Xu, F. Li, T. Wu and Y. Li, *Chem. Eng. J.*, 2016, **296**, 340–348.

41 Y. Sun, Q. Yue, B. Gao, Y. Gao, Q. Li and Y. Wang, *Chem. Eng. J.*, 2013, **217**, 240–247.

42 D. Park, Y. S. Yun and J. M. Park, *J. Colloid Interface Sci.*, 2008, **317**, 54–61.

43 L. Tang, G. D. Yang, G. M. Zeng, Y. Cai, S. S. Li, Y. Y. Zhou, Y. Pang, Y. Y. Liu, Y. Zhang and B. Luna, *Chem. Eng. J.*, 2014, **239**, 114–122.

44 B. Jiang, S. Xin, Y. Liu, H. He, L. Li, Y. Tang, S. Luo and X. Bi, *J. Hazard. Mater.*, 2017, **343**, 1–9.

45 B. Jiang, H. He, Y. Liu, Y. Tang, S. Luo and Z. Wang, *Chemosphere*, 2018, **197**, 367–374.

46 M. J. Dekkers and M. A. A. Schoonen, *Geochim. Cosmochim. Acta*, 1994, **58**, 4147–4153.

47 H. Jabeen, V. Chandra, S. Jung, J. W. Lee, K. S. Kim and S. B. Kim, *Nanoscale*, 2011, **3**, 3583–3585.

48 C. H. Weng, C. P. Huang, H. E. Allen, P. B. Leavens and P. F. Sanders, *Environ. Sci. Technol.*, 1996, **30**, 371–376.

49 B. Jiang, Y. Liu, J. Zheng, M. Tan, Z. Wang and M. Wu, *Environ. Sci. Technol.*, 2015, **49**, 12363–12371.

50 M. Moran, *Colloids Surf., A*, 2004, **244**, 77–85.

51 F. Zhu, L. Li, S. Ma and Z. Shang, *Chem. Eng. J.*, 2016, **302**, 663–669.

52 Z. Ai, Y. Cheng, L. Zhang and J. Qiu, *Environ. Sci. Technol.*, 2008, **42**, 6955–6960.